


Anchor-based optimization of energy density functionals

A. Taninah  and A. V. Afanasjev 

Department of Physics and Astronomy, Mississippi State University, Mississippi 39762, USA

 (Received 24 August 2022; revised 27 February 2023; accepted 14 March 2023; published 3 April 2023)

A new anchor-based optimization method of defining energy density functionals (EDFs) is proposed. In this approach, the optimization of the parameters of EDFs is carried out for a selected set of spherical anchor nuclei, the physical observables of which are modified by the correction function, which takes into account the global performance of EDFs. It is shown that the use of this approach leads to a substantial improvement in the global description of binding energies for several classes of covariant EDFs. The computational cost of defining a new functional within this approach is drastically lower as compared with the one for the optimization which includes the global experimental data on spherical, transitional, and deformed nuclei in the fitting protocol.

DOI: [10.1103/PhysRevC.107.L041301](https://doi.org/10.1103/PhysRevC.107.L041301)

Nuclear density functional theory (DFT) is presently one of the most widely used self-consistent approaches in low-energy nuclear physics [1–4]. It is based on the concept of the energy density functional (EDF), the several parameters of which are defined by the properties of finite nuclei and nuclear matter properties. This approach is universal in a sense that it allows the global description of nuclear properties covering the nuclear landscape from light to very heavy nuclei and from known to unknown nuclei [5,6]. It also provides important information, such as masses, decay and fission rates, etc., for nuclear astrophysics [7,8].

However, the definition of EDFs is not unique and faces a number of challenges, some of which are related to fitting protocols [9,10]. At present, an absolute majority of the EDFs are fitted to the properties of spherical nuclei. This has led to a huge number of functionals, the global performance of which is not established. There are more than 300 relativistic (covariant) EDFs (CEDFs) (see, for example, Ref. [11]) and a comparable number of nonrelativistic Skyrme EDFs. However, such an approach creates a substantial bias towards spherical nuclei: the improvement of the functional for spherical nuclei frequently leads to a degradation of its global performance. Only very limited number of non-relativistic Skyrme and Gogny EDFs and only one CEDF have been fitted globally to experimental data, which includes spherical, transitional and deformed nuclei (see Refs. [12–17]). However, the computational cost of the generation of such functionals is enormous.

In the present paper a new method of anchor-based optimization of the functionals is proposed in order to alleviate these problems. It combines the simplicity of the optimization of EDFs to spherical nuclei with the information on their global performance. In contrast to global fits of EDFs, it typically requires only several rounds of global calculations to achieve a significant improvement of global performance of CEDFs. This was verified for several classes of CEDFs and is achieved at a moderate increase of computational time as compared with the optimization to only spherical nuclei.

The general procedure for the anchor-based optimization of EDFs is the following:

- (1) The set of “anchor” spherical nuclei is selected and the optimization of the functional is carried out with spherical relativistic Hartree-Bogoliubov (RHB) computer code using experimental data on these nuclei and nuclear matter properties (NMP) (see Refs. [6,18] and Supplemental Material [19] for details). The obtained functional is labeled as EDF_i ($i = 0$). Here i is the counter of the iteration in the anchor-based optimization.
- (2) Global calculations of the masses, charge radii and other physical observables are carried out with axially deformed RHB code using EDF_i for the set of nuclei in which respective experimental data exist. The set of binding energies $E_{EDF_i}(Z, N)$ is defined for n even-even nuclei, the masses of which have been either measured or estimated in the AME2016 mass evaluation [20]. Note that this set of the nuclei includes spherical, transitional, and deformed nuclei.
- (3) The correction function

$$E_{\text{corr}}(Z, N) = \alpha_i(N - Z) + \beta_i(N + Z) + \gamma_i \quad (1)$$

is added¹ to the obtained set of calculated binding energies:

$$E_{\text{pseudo}}(Z, N) = E_{EDF_i}(Z, N) + E_{\text{corr}}(Z, N). \quad (2)$$

Then, the optimal parameters α_i , β_i and γ_i are determined by minimizing ΔE_{rms} defined as:

$$\Delta E_{\text{rms}} = \sqrt{\frac{\sum_{k=1}^n [E_{\text{pseudo}}(Z, N) - E_{\text{exp}}(Z, N)]^2}{n}}, \quad (3)$$

¹Alternative functional dependencies have been explored. However, Eq. (1) brings the best improvement of the EDFs.

where $E_{\text{exp}}(Z, N)$ is experimental binding energy of the k th nucleus with (Z, N) and k runs over all even-even nuclei for which experimental data exist. Thus, the addition of $E_{\text{corr}}(Z, N)$ to binding energies aims at the minimization of global difference between calculated and experimental binding energies. The variation of the parameters α_i , β_i , and γ_i with iteration number during the iterative procedure are illustrated in Tables 1–3 of the Supplemental Material [19].

- (4) The energies of spherical anchor nuclei are redefined as

$$E_{\text{exp}}^{\text{pseudo}}(Z, N) = E_{\text{exp}}(Z, N) + E_{\text{corr}}(Z, N), \quad (4)$$

where $E_{\text{corr}}(Z, N)$ is calculated for optimal parameters α_i , β_i , and γ_i defined in the previous step. A new set of parameters EDF $_{i+1}$ is defined using $E_{\text{exp}}^{\text{pseudo}}(Z, N)$ as “experimental” data and the procedure of point 1.

- (5) New global calculations are carried out using EDF $_{i+1}$ and the procedure of point 2. A significant improvement in the global description of masses has been achieved at the first step of the iterative procedure for the DD-MEY, NL5(Y), and PC-Y functionals and at third step for the DD-MEX1 one.² Further repetition of steps 3–5 leads to only moderate improvement of the global description of the masses.

The convergence of the iterative procedure is reached in the limit $\alpha_i \rightarrow 0$, $\beta_i \rightarrow 0$, and $\gamma_i \rightarrow 0$. However, the analysis presented in Tables 1–3 of the Supplemental Material [19] clearly suggests that the termination of the iterative procedure before reaching this limit may lead to only very small (if any) degradation of the global description of masses.

The spherical and deformed calculations are carried out using the RHB computer codes developed in Refs. [6,18]. The truncation of the basis is performed in such a way that all states belonging to the major shells up to $N_F = 20$ fermionic shells for the Dirac spinors and up to $N_B = 20$ bosonic shells for the meson fields are taken into account. Note that the latter applies only to the functionals which contain meson exchange such as those belonging to nonlinear meson coupling (NLME) and density dependent meson-nucleon coupling (DDME) classes of the functionals (see Refs. [6,18]). The accuracy of the truncation of the basis is discussed in the Supplemental Material [19].

In order to avoid the uncertainties connected with the definition of the size of the pairing window, the separable form of the finite range Gogny pairing interaction introduced by Tian *et al.* [24] is used with two versions of the strength f of the pairing. In the first one (called further “Pair 1”), the pairing strength is dependent on proton number (see Ref. [6] for detail). In the second one called “Pair 2” (see Ref. [25] for detail), the proton pairing is made mass dependent via

$$f_{\pi} = 1.877(N + Z)^{-0.1072}, \quad (5)$$

and neutron pairing is isospin dependent via

$$f_{\nu} = 1.208e^{-0.674 \frac{N-Z}{N+Z}}. \quad (6)$$

This type of phenomenological scaling of pairing strength provides the best reproduction of the experimental pairing indicators (see Ref. [25]). Note that the labels of the functionals defined with Pair 2 pairing contain the letter “Y” at/near their end.

The anchor-based optimization method is applied here for the DDME, NLME, and point coupling (PC) classes of CEDFs (see Refs. [10,18] and the Supplemental Material [19] for technical details). For each class, the functionals with the best global performance such as DD-ME2 [22], NL5(E) [10], and PC-PK1 [23] are used as a starting point. In addition, the basic features of their fitting protocols are employed here. As a consequence, there are 12 anchor spherical nuclei in the DDME and NLME models and 60 anchor spherical nuclei in the PC model. The types of the input data for the fitting protocols and related adopted errors are summarized in Table 4 of the Supplemental Material [19].

The optimization of the CEDFs in spherical nuclei is performed in the following way. First, approximately 200 trials of minimization from the sets of initial parameters, randomly generated in a large parameter hyperspace, are performed using the simplex based minimization method. Second, the minimization is repeated by using initial parameters generated in smaller parameter hyperspaces around several local minima characterized by the lowest penalty functions using both simplex-based and simulated annealing³ minimization methods. This procedure guarantees the convergence to the global minimum and provides information on parametric correlations between the parameters of CEDFs (see Ref. [18]).

The global performance of existing [DD-ME2, NL5(E) and PC-PK1] and new [DD-MEX1, DD-MEX2, DD-MEY, NL5(Y), PC-Y and PC-Y1] functionals obtained by means of anchor-based optimization method are summarized in Table I. When considering the quality of the functionals one should take into account the ranges of the nuclear matter properties (NMPs) recommended for relativistic functionals in Ref. [11]. These are $\rho_0 \approx 0.15 \text{ fm}^{-3}$, $E/A \approx -16 \text{ MeV}$, $K_0 = 190\text{--}270$, $J = 25\text{--}35 \text{ MeV}$ ($J = 30\text{--}35 \text{ MeV}$) and $L_0 = 25\text{--}115$ ($L_0 = 30\text{--}80$) for the SET2a (SET2b) sets of the constraints on the experimental/empirical ranges for the quantities of interest.

The DD-MEX1 functional originates from the DD-ME2 one: both have the same fitting protocol (see Supplemental Material [19]) but the CEDF DD-ME2 is fitted at the BCS level employing monopole pairing while the DD-MEX1 one is fitted at the RHB level with the Pair 1 separable pairing. However, the DD-MEX1 functional, fitted with the anchor-based optimization method, provides a substantial improvement in the global description of binding energies (from $\Delta E_{\text{rms}} = 2.436 \text{ MeV}$ for DD-ME2 down to $\Delta E_{\text{rms}} = 1.651 \text{ MeV}$ for DD-MEX1; see Table I). It also provides a slight improvement

²This feature of the anchor based optimization method can be extremely useful for theoretical groups with limited computational resources.

³It is our experience that the simulated annealing method is extremely costly and numerically unstable for large parameter hyperspaces.

TABLE I. The rms deviations ΔE_{rms} , $\Delta(S_{2n})_{\text{rms}}$, $\Delta(S_{2p})_{\text{rms}}$, and $\Delta(r_{\text{ch}})_{\text{rms}}$ between calculated and experimental binding energies E , two-neutron (two-proton) separation energies S_{2n} (S_{2p}), and charge radii r_{ch} . The first three observables are determined with respect to a “measured + estimated” set of experimental masses of 855 even-even nuclei from the AME2016 mass evaluation [20]. The $\Delta(r_{\text{ch}})_{\text{rms}}$ values are calculated using experimental data on charge radii of 305 even-even nuclei from Ref. [21]. The values shown in parentheses are the rms deviations for the subset of nuclei which excludes light nuclei with $A < 70$. The incompressibility K_0 , the symmetry energy J , and the slope L_0 of the symmetry energy of the functionals under study are shown in columns 6, 7, and 8, respectively.

1	ΔE_{rms} (MeV)	$\Delta(S_{2n})_{\text{rms}}$ (MeV)	$\Delta(S_{2p})_{\text{rms}}$ (MeV)	$\Delta(r_{\text{ch}})_{\text{rms}}$ (fm)	K_0 (MeV)	J (MeV)	L_0 (MeV)
	2	3	4	5	6	7	8
DD-ME2 [22]	2.436 (2.300)	1.056 (0.854)	0.949 (0.750)	0.0266 (0.0262)	250.9	32.9	49.4
DD-MEX [18]	2.849 (2.963)	1.095 (0.972)	0.978 (0.847)	0.0247 (0.0249)	267.0	32.9	47.8
DD-MEX1	1.637 (1.539)	1.045 (0.873)	0.896 (0.704)	0.0261 (0.0263)	291.8	32.5	51.8
DD-MEX2	2.236 (1.791)	1.228 (0.913)	1.271 (0.928)	0.0466 (0.0488)	255.8	35.9	85.3
DD-MEY	1.734 (1.414)	1.259 (0.876)	1.026 (0.755)	0.0264 (0.0244)	265.8	32.8	51.8
NL5(E) [10]	2.802 (2.689)	1.204 (0.864)	1.366 (1.033)	0.0285 (0.0271)	253.0	38.9	125.0
NL5(Y)	2.362 (1.675)	1.256 (0.709)	1.222 (0.772)	0.0297 (0.0292)	254.5	36.6	116.7
PC-PK1 [23]	2.400 (2.149)	1.331 (0.932)	1.354 (0.875)	0.0306 (0.0269)	238	35.6	113
PC-Y	1.951 (1.600)	1.438 (0.770)	1.175 (0.690)	0.0311 (0.0247)	241	35.1	105
PC-Y1	1.849 (1.509)	1.345 (0.846)	1.106 (0.822)	0.0294 (0.0249)	240	34.9	107

in the description of two-neutron and two-proton separation energies and charge radii. Most of the NMPs of this functional are within the SET2b limits: the only exception is incompressibility K_0 which exceeds the SET2b upper limit.

It is interesting to see whether the binding energies and charge radii alone can provide a reasonable constraint on NMPs and neutron skins. For that, the DD-MEX2 and DD-MEY functionals have been created, the fitting protocols of which do not contain any information on NMPs and neutron skins (see Table 4 in the Supplemental Material [19]). In addition, the adopted errors for binding energies are fixed at 1.0 MeV for all nuclei in this class of functionals. The DD-MEX2 functional has been optimized with the Pair 1 separable pairing. As compared with DD-ME2 (DD-MEX1) it leads to some improvement (degradation) in the description of binding energies but provides less accurate description of two-proton and two-neutron separation energies and charge radii as compared with the two above-mentioned functionals (see Table I).

The situation drastically improves when the Pair 2 separable pairing is used. This leads to the DD-MEY functional, which provides the second best global description of binding energies ($\Delta E_{\text{rms}} = 1.734$ MeV) and the best description of the binding energies of the $A > 70$ nuclei ($\Delta E_{\text{rms}} = 1.414$ MeV) among considered functionals (see Table I). Despite the fact that the DD-MEY functional was fitted without constraint on NMPs, they are within the SET2b limits (see Table I). In particular, it gives a more reasonable value of incompressibility K_0 than the DD-MEX1 functional. These facts potentially indicate the importance of the isospin dependent neutron pairing in the simultaneous description of binding energies and NMP. However, the description of two-neutron and two-proton separation energies with this functional is somewhat worse than in the DD-MEX1 one.

To verify the results obtained with anchor based optimization method we also employed the method of minimization of Ref. [26], which is used in nuclear mass table fits by the Brussels group. In this method, the binding

energies of deformed and transitional nuclei are corrected by the deformation energies so the optimization is carried out for the energies of spherical solution of the nuclei used in the fitting protocol. In a given nucleus, the deformation energy represents the difference between the energy of the global minimum with deformations $\beta_i \neq 0$ ($i = 2, 4, \dots$) and that of the spherical solution with $\beta_i = 0$. Because of available computers we used 400 even-even nuclei evenly spread over nuclear chart (starting from actinides and going down to light nuclei and eliminating each second even-even nucleus) in these calculations. The iterative procedure in this method requires new calculations of deformation energies at each iteration (see Ref. [26] for details) and it turns out that their convergence is quite slow, especially in the DD-MEX1 type of the functional. The rms deviations between experimental and calculated binding energies ΔE_{rms} obtained in these calculations are $1.672(0.068)^4$ and $1.613(0.258)$ MeV for the DD-MEY and DD-MEX1 functionals, respectively. Thus, the results obtained with this approach are in line with those obtained in anchor based optimization approach (see Table I); some difference in the results are due to different selection of the nuclei directly included in the fitting protocol. Note that this approach is numerically substantially more time consuming as compared with the anchor based optimization approach because (i) substantially more “spherical” nuclei (400 versus 12) are used in the minimization procedure and (ii) there is slow convergence of deformation energies in the iterative procedure.

The anchor-based optimization method has been applied also to the NLME and PC classes of the CEDFs. In both cases, it leads to an improvement of global description of masses. The NL5(E) functional (see Ref. [10]) is the starting point for

⁴The numbers shown in parentheses are the errors in deformation energies due to limited number of iterations in the iterative procedure.

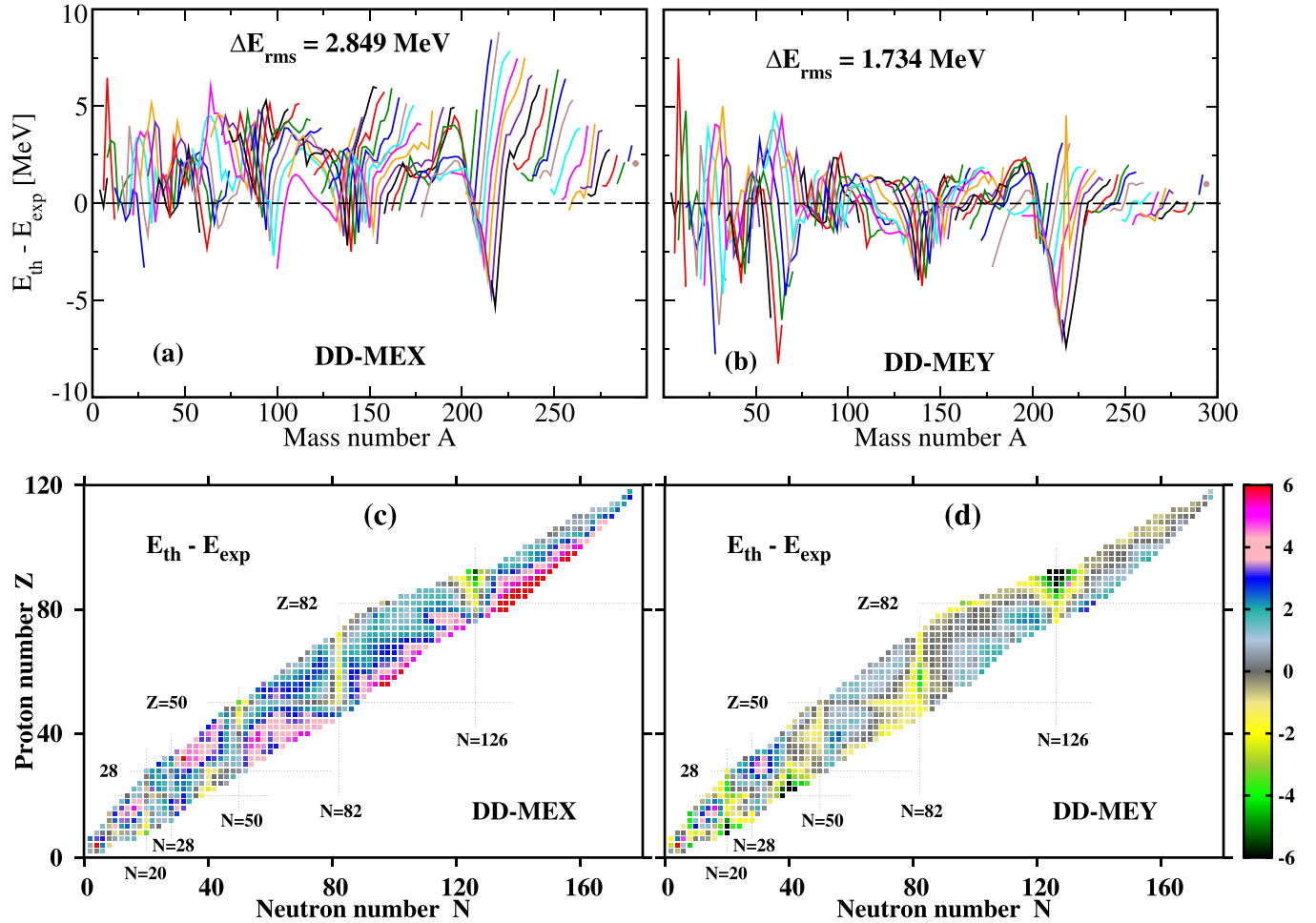


FIG. 1. The differences $E_{\text{th}} - E_{\text{exp}}$ between calculated (E_{th}) and experimental (E_{exp}) masses for indicated CEDFs. All 855 even-even nuclei for which measured and estimated masses are available in the AME2016 compilation [20] are used in this comparison. If $E_{\text{th}} - E_{\text{exp}} < 0$, the nucleus is more bound in the calculations than in experiment.

the optimization of the NL5(Y) CEDF. Note that the Pair 1 and Pair 2 separable pairings are used in the fitting protocols of the NL5(E) and NL5(Y) CEDFs, respectively. Table I shows that the application of the anchor based optimization method in combination with the use of isospin dependent neutron pairing leads to a substantial improvement of global mass description and some improvement of the symmetry energy J and the slope of the symmetry energy L_0 . The same situation exists also for the PC functionals. The anchor based optimization starting from the PC-PK1 functional leads to the CEDF PC-Y, which provides a substantial improvement of the global description of binding energies (see Table I).

Note that the fitting protocols of the above-mentioned DDME and NLME functionals include only 12 spherical anchor nuclei. For these functionals it was verified that the increase of the number of spherical anchor nuclei to 60 (as in the fitting protocol of the PC-PK1 functional [23]) does not lead to an improvement of the global description of binding energies. The same conclusion is valid for the PC model: the reduction of the number of the anchor spherical nuclei from 60 in the PC-Y functional down to 12 in the PC-Y1 functional (see Table 1 in the Supplemental Material [19]) leads to some

improvement in the description of physical observables (see Table I).

With the exception of the DD-MEX2 functional all CEDFs shown in Table I give comparable rms deviations for charge radii $\Delta(r_{\text{ch}})_{\text{rms}} \approx 0.026$ fm, corresponding to a high precision of $\approx 0.5\%$ in charge radii predictions. These results and the analysis of Ref. [27] suggest that the inclusion of global data on charge radii will not likely lead to an appreciable improvement of the functionals.

Figure 1 illustrates the improvements in the global description of the masses and related physical observables when the anchor-based optimization method is employed. DD-MEX is the best DDME functional as defined by the penalty function of the fitting protocol including only spherical nuclei (see Ref. [18]). However, this bias towards spherical nuclei leads to $\Delta E_{\text{rms}} = 2.849$ MeV in the global description of the masses (see Table I) and appreciable deviations between theory and experiment displayed in Figs. 1(a) and 1(c). In particular, it leads to a systematic shift of the average $E_{\text{th}} - E_{\text{exp}}$ values from the $E_{\text{th}} - E_{\text{exp}} = 0$ line [see Fig. 1(a)]. In contrast, such a shift does not appear for the DD-MEY functional [see Fig. 1(a)] which, in addition, improves the description

of isospin dependence of the $E_{\text{th}} - E_{\text{exp}}$ values [compare Figs. 1(c) and 1(d)].

Note that these improvements are obtained by a larger emphasis on medium and heavy mass nuclei with $A > 70$ in the anchor-based optimization method. For these nuclei a substantial improvement in the description of the masses and two-particle separation energies is obtained [see Table I and compare Figs. 1(a) and 1(b) and Figs. 1(c) and 1(d)]. In contrast, the spreads in the $E_{\text{th}} - E_{\text{exp}}$ values are getting larger for the light ($A < 70$) nuclei [compare Figs. 1(a) and 1(b)]. However, this is not critical since beyond-mean-field effects are expected to be larger in light ($A < 70$) nuclei as compared with heavier ones. This is in line with the observation that the accuracy of the description of the masses and two-particle separation energies improves substantially when light $A < 70$ nuclei are excluded from the analysis (see Table I). This improvement is especially drastic for the DD-MEX1, DD-MEX2, DD-MEY, NL5(Y), PC-Y, and PC-Y1 functionals defined by the anchor-based optimization method.

It is interesting to compare the performance of these functionals with those obtained in Skyrme DFT for the UNEDF* class of the functionals, which, similarly to our approach, has been defined at the mean field level without inclusion of rotational and vibrational correlations. The UNEDF0 [14], UNEDF1 [15], and UNEDF2 [28] EDFs were optimized by fitting their parameters to large (but restrictive) sets of experimental data involving spherical and deformed nuclei. These EDFs describe globally nuclear masses with $\Delta E_{\text{rms}} = 1.428$ MeV (UNEDF0), 1.912 MeV (UNEDF1), and 1.950 MeV (UNEDF2). These values are close to those obtained with the DD-MEX1, DD-MEY, PC-Y, and PC-Y1 CEDFs, but numerical cost of the optimization of these Skyrme EDFs is drastically larger than that in the anchor-based optimization method.

In conclusion, a new anchor-based optimization method of defining the energy density functionals has been proposed. It combines the simplicity of the fitting of EDFs

to spherical nuclei with global information on the reproduction of experimental masses by EDFs. This is done by correcting the binding energies of the anchor spherical nuclei used in optimization. As a consequence, the computational cost of defining a new functional is drastically lower as compared with alternative methods of optimization which simultaneously include the experimental data on spherical and deformed nuclei. Despite that, the global performance of the functionals defined by the anchor-based optimization method becomes comparable with the one obtained for the UNEDF* class of nonrelativistic Skyrme functionals. Although the anchor-based method is applied here for CEDFs, it can also be used for non-relativistic Skyrme and Gogny functionals.

The functionals studied in the present paper are restricted to the ones defined at the mean field level. However, the anchor-based optimization method can be easily generalized to approaches which include correlations beyond mean field. For that the RHB approach in the point 2 of the anchor-based optimization method procedure has to be replaced by an appropriate beyond-mean field-method (such as a five-dimensional collective Hamiltonian [29–31]).⁵ This will allow one to bypass the existing challenge of extreme computational cost of fitting EDFs at the beyond-mean-field level and generate such functionals. It is reasonable to expect that they will lead to a further improvement of the description of binding energies (see, for example, Refs. [34,35]).

Note that, in addition to the references directly cited in the main body of the paper, the Supplemental Material [19] provides citations to Refs. [36–44].

⁵Alternatively, one can use a more simplistic approach and add phenomenological rotational corrections to the binding energies calculated in the RHB or similar nonrelativistic approach; this is done in a number of the calculations of masses (see, for example, Refs. [32–34]).

-
- [1] M. Bender, P.-H. Heenen, and P.-G. Reinhard, *Rev. Mod. Phys.* **75**, 121 (2003).
 - [2] D. Vretenar, A. V. Afanasjev, G. A. Lalazissis, and P. Ring, *Phys. Rep.* **409**, 101 (2005).
 - [3] J. E. Drut, R. J. Furnstahl, and L. Platter, *Prog. Part. Nucl. Phys.* **64**, 120 (2010).
 - [4] S. Peru and M. Martini, *Eur. Phys. J. A* **50**, 88 (2014).
 - [5] J. Erler, N. Birge, M. Kortelainen, W. Nazarewicz, E. Olsen, A. M. Perhac, and M. Stoitsov, *Nature (London)* **486**, 509 (2012).
 - [6] S. E. Agbemava, A. V. Afanasjev, D. Ray, and P. Ring, *Phys. Rev. C* **89**, 054320 (2014).
 - [7] M. Arnould and S. Goriely, *Prog. Part. Nucl. Phys.* **112**, 103766 (2020).
 - [8] J. J. Cowan, C. Sneden, J. E. Lawler, A. Aprahamian, M. Wiescher, K. Langanke, G. Martínez-Pinedo, and F.-K. Thielemann, *Rev. Mod. Phys.* **93**, 015002 (2021).
 - [9] J. Dobaczewski, W. Nazarewicz, and P.-G. Reinhard, *J. Phys. G: Nucl. Part. Phys.* **41**, 074001 (2014).
 - [10] S. E. Agbemava, A. V. Afanasjev, and A. Taninah, *Phys. Rev. C* **99**, 014318 (2019).
 - [11] M. Dutra, O. Lourenco, S. S. Avancini, B. V. Carlson, A. Delfino, D. P. Menezes, C. Providencia, S. Typel, and J. R. Stone, *Phys. Rev. C* **90**, 055203 (2014).
 - [12] S. Goriely, N. Chamel, and J. M. Pearson, *Phys. Rev. Lett.* **102**, 152503 (2009).
 - [13] S. Goriely, N. Chamel, and J. M. Pearson, *Phys. Rev. C* **88**, 061302(R) (2013).
 - [14] M. Kortelainen, T. Lesinski, J. Moré, W. Nazarewicz, J. Sarich, N. Schunck, M. V. Stoitsov, and S. Wild, *Phys. Rev. C* **82**, 024313 (2010).
 - [15] M. Kortelainen, J. McDonnell, W. Nazarewicz, P.-G. Reinhard, J. Sarich, N. Schunck, M. V. Stoitsov, and S. M. Wild, *Phys. Rev. C* **85**, 024304 (2012).
 - [16] S. Goriely, S. Hilaire, M. Girod, and S. Péru, *Phys. Rev. Lett.* **102**, 242501 (2009).
 - [17] D. Peña-Arteaga, S. Goriely, and N. Chamel, *Eur. Phys. J. A* **52**, 320 (2016).

- [18] A. Taninah, S. E. Agbemava, A. V. Afanasjev, and P. Ring, *Phys. Lett. B* **800**, 135065 (2020).
- [19] See Supplemental Material at <http://link.aps.org/supplemental/10.1103/PhysRevC.107.L041301> for the details of the fitting protocols, the numerical values of the parameters of covariant energy density functionals, and the discussion of truncation errors.
- [20] M. Wang, G. Audi, F. G. Kondev, W. Huang, S. Naimi, and X. Xu, *Chin. Phys. C* **41**, 030003 (2017).
- [21] I. Angeli and K. P. Marinova, *At. Data Nucl. Data Tables* **99**, 69 (2013).
- [22] G. A. Lalazissis, T. Nikšić, D. Vretenar, and P. Ring, *Phys. Rev. C* **71**, 024312 (2005).
- [23] P. W. Zhao, Z. P. Li, J. M. Yao, and J. Meng, *Phys. Rev. C* **82**, 054319 (2010).
- [24] Y. Tian, Z. Y. Ma, and P. Ring, *Phys. Lett. B* **676**, 44 (2009).
- [25] S. Teeti and A. V. Afanasjev, *Phys. Rev. C* **103**, 034310 (2021).
- [26] F. Tondeur, S. Goriely, J. M. Pearson, and M. Onsi, *Phys. Rev. C* **62**, 024308 (2000).
- [27] U. C. Perera, A. V. Afanasjev, and P. Ring, *Phys. Rev. C* **104**, 064313 (2021).
- [28] M. Kortelainen, J. McDonnell, W. Nazarewicz, E. Olsen, P.-G. Reinhard, J. Sarich, N. Schunck, S. M. Wild, D. Davesne, J. Erler, and A. Pastore, *Phys. Rev. C* **89**, 054314 (2014).
- [29] T. Nikšić, Z. P. Li, D. Vretenar, L. Próchniak, J. Meng, and P. Ring, *Phys. Rev. C* **79**, 034303 (2009).
- [30] Z. P. Li, T. Nikšić, D. Vretenar, J. Meng, G. A. Lalazissis, and P. Ring, *Phys. Rev. C* **79**, 054301 (2009).
- [31] Z. Shi, A. V. Afanasjev, Z. P. Li, and J. Meng, *Phys. Rev. C* **99**, 064316 (2019).
- [32] P. Möller, J. R. Nix, W. D. Myers, and W. J. Swiatecki, *At. Data Nucl. Data Tables* **59**, 185 (1995).
- [33] S. Goriely, M. Samyn, and J. M. Pearson, *Phys. Rev. C* **75**, 064312 (2007).
- [34] Q. S. Zhang, Z. M. Niu, Z. P. Li, J. M. Yao, and J. Meng, *Front. Phys.* **9**, 529 (2014).
- [35] Y. L. Yang, Y. K. Wang, P. W. Zhao, and Z. P. Li, *Phys. Rev. C* **104**, 054312 (2021).
- [36] T. Nikšić, N. Paar, D. Vretenar, and P. Ring, *Comput. Phys. Commun.* **185**, 1808 (2014).
- [37] A. V. Afanasjev, J. König, and P. Ring, *Nucl. Phys. A* **608**, 107 (1996).
- [38] S. E. Agbemava, A. V. Afanasjev, A. Taninah, and A. Gyawali, *Phys. Rev. C* **99**, 034316 (2019).
- [39] T. Nikšić, D. Vretenar, and P. Ring, *Phys. Rev. C* **78**, 034318 (2008).
- [40] G. A. Lalazissis, S. Karatzikos, R. Fossion, D. Pena Arteaga, A. V. Afanasjev, and P. Ring, *Phys. Lett. B* **671**, 36 (2009).
- [41] D. Adhikari, H. Albataineh, D. Androic, K. Aniol, D. S. Armstrong, T. Averett, C. Ayerbe Gayoso, S. Barcus, V. Bellini, R. S. Beminiwattha, J. F. Benesch, H. Bhatt, D. Bhatta Pathak, D. Bhetuwal, B. Blaikie, Q. Campagna, A. Camsonne, G. D. Cates, Y. Chen, C. Clarke *et al.* (PREX Collaboration), *Phys. Rev. Lett.* **126**, 172502 (2021).
- [42] D. Adhikari, H. Albataineh, D. Androic, K. A. Aniol, D. S. Armstrong, T. Averett, C. Ayerbe Gayoso, S. K. Barcus, V. Bellini, R. S. Beminiwattha, J. F. Benesch, H. Bhatt, D. Bhatta Pathak, D. Bhetuwal, B. Blaikie, J. Boyd, Q. Campagna, A. Camsonne, G. D. Cates, Y. Chen *et al.* (CREX Collaboration), *Phys. Rev. Lett.* **129**, 042501 (2022).
- [43] M. C. Atkinson, M. H. Mahzoon, M. A. Keim, B. A. Bordelon, C. D. Pruitt, R. J. Charity, and W. H. Dickhoff, *Phys. Rev. C* **101**, 044303 (2020).
- [44] B. Hu, W. Jiang, T. Miyagi, Z. Sun, A. Ekström, C. Forssén, G. Hagen, J. D. Holt, T. Papenbrock, S. R. Stroberg, and I. Vernon, *Nat. Phys.* **18**, 1196 (2022).